Quantitative assessment of rat bone regeneration using complex master–slave optical coherence tomography

Ruxandra LUCA,[a] Carmen Darinca TODEA,[a,*] Virgil-Florin DUMA,[b,c,*] Adrian BRADU,[d] Adrian Gh. PODOLEANU[d]

[a] 'Victor Babes' University of Medicine and Pharmacy of Timisoara, School of Dental Medicine, 2 Eftimie Murgu Place, Timisoara, Romania, 300041

[b] 'Aurel Vlaicu' University of Arad, 3OM Optomechatronics Group, 77 Revolutiei Ave., Arad, Romania, 310130

[c] Polytechnic University of Timisoara, Doctoral School, Timisoara, Romania, 300222

[d] University of Kent, School of Physical Sciences, Canterbury, UK, CT2 7NH

*These two are both correspondence authors.

Address all correspondence to:

Prof. Dr.-habil. Virgil-Florin Duma,

3OM Optomechatronics Group, Faculty of Engineering, 'Aurel Vlaicu' University of Arad

77 Revolutiei Ave., Arad 310130, Romania;

Tel: +40-751-511451; Email: duma.virgil@osamember.org

Running title: Quantitative assessment of rat bone regeneration using complex master–slave OCT

Abstract.

Background. The need for hard and soft tissues in oral implantology determined the development of methods and techniques to increase bone volume and their quality with different alternative materials used as substituents of patient's natural bone. In addition, laser radiation can be used to accelerate the repair of fractures and to produce an increased volume of formed callus, as well as an increase in bone mineral density. **Method.** The aim of this work is to evaluate the capability of an in-house developed multimodal Complex Master Slave (CMS) enhanced Swept Source (SS) OCT imaging instrument to analyze the increase in the quantity and quality of newly-formed bone using low level laser therapy (LLLT). Bone formation is quantitatively assessed in 5 mm cylindrical defects made in the calvaria part of the skull of living rats. Samples are divided in three study groups: (A) a negative control group, for which the natural healing process of the defect is investigated, (B) a positive control group, for which bovine graft is used to stimulate bone formation, and (C) a study group, in which both bovine graft is added to the created defect and LLLT is applied throughout the entire healing period. The animals are sacrificed after 14, 21, and 30 days, and the samples imaged using the multimodal imaging CMS/SS-OCT instrument. **Results.** The method allows for the simultaneous monitoring of the bone tissue via two cross-sections and nine *en face* images taken at adjustable depths into the sample. A global image with course axial resolution allows for the positioning of the field-of-view of the system on the area of interest on the tissue. The quantitative assessment of the process of bone formation is completed using the differences in brightness between the native bone, the artificial bone graft, and the newly formed bone. **Conclusions.** Group C is demonstrated to have a higher volume of formed bone than Group B, which had more new bone

than Group A. By analyzing the evolution of this volume of new bone in time, the most significant difference was after 21 days, therefore approximately after two thirds of the total time interval analyzed. After 30 days, the volumes of bone tend to move closer, as they begin to fill the available gap. The study demonstrates that OCT can assess quantitatively the positive impact of LLLT on bone regeneration.

Keywords: optical coherence tomography (OCT), oral implantology, bone formation, low level laser therapy (LLLT), *en face* imaging.

1 Introduction

Alveolar ridge resorption subsequent to the loss of tooth is a common phenomenon. Immediately after the extraction of a tooth, alveolar ridge width and height decrease rapidly, with a loss of about 40 to 60% of their values in the first three years after extraction. Then, this percentage drops by 0.25 to 0.5% per year. The decrease in blood supply, the localized inflammatory process, and the pressure from various types of prosthetic restorations can lead to alveolar bone resorption [1].

The requirements to provide the patient with a complex implant treatment increased considerably over the last few years, therefore the development of bone augmentation techniques to increase the bone volume prior to placing implants and prosthetic restorations has become a hot topic in dentistry [2]. Oral rehabilitation of partial or total edentulous patients with dental implants has become a routine treatment in recent decades, with long-term sustainable results. However, local unfavorable conditions pertaining to the bone atrophy, periodontal disease, or sequelae after trauma provide insufficient bone volume or unfavorable vertical, horizontal, and sagittal inter-

maxillary relationships, hence difficulties to place implants or in an incorrect placement from a functional and aesthetical point of view [3].

The need for hard and soft tissues in the oral implantology field lead to the development of methods and techniques to increase bone volumes and their quality. Bone graft is the second most common transplantable tissue, with blood being by far the most common [4,5]. The gold standard of bone grafting is harvesting autologous cortical and cancellous bone from the iliac crest (i.e., auto-grafting). Although it provides optimal osteoconductive, osteoinductive, and osteogenetic properties, autografting has its limitations, as it can lead to complications. Therefore, currently, other available alternative materials are utilized as a substituent of the patient's natural bone, such as alloplastic grafts (synthetic) or xenograft (animal origin materials) during common procedures, such as guided bone regeneration and osteodistraction. Synthetic materials tend to be used as bone grafts more often, because of their advantages, including the absence of contamination, good bioavailability, ease of handling, and good patient acceptance.

The strategy used in bone tissue engineering involves using a suitable scaffold, which can act as a template for cell interactions, providing a structural support for the newly formed bone tissue [6]. Due to its similarity to human bone and its benefits related to availability and ease of surgical technique [7,8], this scaffold shows osteoconductive properties when it is in close contact with the newly formed bone [9].

Due to the positive effects of laser radiation on bone metabolism, as observed especially in the consolidation of fractures, laser photobiomodulation (*low level laser energy therapy* - LLLT) has been extended to clinical practice [3]. Renno et al. [10] and Stein et al. [11] showed a significant increase in the proliferation of osteoblasts after irradiation with energy from a diode laser emitting 20 J/cm^2 at a wavelength of 830 nm. In addition, laser radiation seems to accelerate the

repair of fractures and produces an increased volume of formed callus, as well as an increase in bone mineral density. Other effects related to the use of LLLT include an increased blood supply, the enhancement of the activity of osteoblasts, the organization of collagen fibers, and changes in the intracellular mitochondrial adenosine triphosphate. LLLT is a noninvasive method that stimulates bone formation and accelerates the healing of bone defects [12-14]. LLLT can stimulate bone cellular proliferation [15], reflecting in osteoblastic activity, and can also increase intracellular calcium level [16].

Although a significant number of research papers on LLLT have been already published, its mechanism is poorly understood [17]. Studies have suggested a positive effect of LLLT on bone healing either *in vivo* [18] or *in vitro* [19], although they did not find any effect of LLLT on the repair of soft or mineralized tissues [20]. First, these inconsistent reports may be attributed to the wide variety of laser types and setups that have been utilized in different studies. Second, the true mechanism that leads to a positive effect of laser light on different tissues is not fully understood because of the diversity of techniques, methods, and experimental models, as well as the variety of treatment protocols reported [21]. These aspects make the comparative analysis of the results obtained so far difficult.

Several hypotheses have been suggested. The conflicting results of LLLT on bio-modulation are considered to be mainly related to the diversity of the radiation parameters: treatment dose, power density, number of applications, method of applying, and laser wavelength [22]. For the latter parameter, it has been shown that tissue response is altered with regard to the wavelength used as follows: the radiation corresponding to the red wavelengths shows an activation of the mitochondrial respiratory chain components, resulting in the initiation of a cascade of cellular reactions, whereas in the region of the infrared light, there is an activation of chromophores

located in the cellular membrane [23]. It is considered that the main effect of LLLT occurs in mitochondria. Previous studies demonstrated that irradiated fibroblasts produced a greater amount of collagen. On the same reasoning, other studies considered that osteoblasts irradiated with laser will be stimulated to osteoid matrix formation. From the clinical point of view, these events translate into mature, more bone deposit [24], that satisfy the needs of prosthetic implant restorations.

The most frequent methods utilized to evaluate bone remodeling after LLLT are represented by densitometric analysis [25], histopathological and histomorphometrical analysis [26], scanning electron microscopy (SEM), plain radiographs, and biomechanical analysis. Recently, micro-computed tomography (micro-CT) has been performed to observe the bone regeneration over an entire defect site. Using a computer program to convert micro-CT images to three-dimensional (3D)/volumetric reconstructions, the entire bone regenerated in the defects can be observed [27].

Despite the variety of instruments listed above, there is a need for a tool simultaneously efficient and non-invasive, and that can present sufficient resolution to evaluate the bone healing process. Optical Coherence Tomography (OCT) [28,29] is such an investigation technique that is more and more applied in dentistry as a promising tool [30], after being initially developed for ophthalmology. Nowadays, OCT has a multitude of biomedical applications, from ophthalmology [28,31] to skin [32], oral cavity [33-36], and endoscopy [37]. Whilst in dental medicine OCT has been used to study both soft and hard tissue, as well as different dental constructs [35,38], a few studies exist only, to our knowledge, on using OCT for assessment of bone regeneration. These studies include: (i) evaluation of the effects of sterilization through ionizing radiation on the bone matrix from the tissue banks used as allograft [39,40]; (ii) imaging early osteoarthritis, identifying changes prior to cartilage thinning both *in vitro* and *in vivo* in

patients and in osteoarthritis animal models identifying early rheumatoid arthritis and guiding tendon repair [41]; (iii) 3D imaging of the tissue at the implant sites for *in vitro* investigations, for which OCT images obtained at 1325 nm showed significant contrast and spatial resolution to study osseointegration of implants in the maxilla at a 200 μm depth inside the bone [42,43]. In bone regeneration assessment, we have utilized both the capability of OCT and micro-CT to evaluate the bone grafting material/bone interface [44].

The aim of the present study is to evaluate the capability of a multimodal Complex Master Slave (CMS) enhanced Swept Source (SS) OCT imaging instrument to provide reliable information on the bone regeneration process. Due to the importance and potential impact of bone regeneration, as pointed out above, we approach *ex vivo* samples of rat calvarial defects which underwent different protocols of bone augmentation, as well as bone augmentation due to LLLT.

The remaining of this paper is structured as follows: Section 2 describes the protocols of bone preparation and the in-house developed CMS/SS OCT instrument. Results are discussed in Section 3, while Section 4 concludes the study and provides directions of future work, from both points of view, of bone regeneration and of the OCT technique employed for this study.

2 Materials and methods

2.1 Preparation of bone samples

The ethical approval for the preparation of bone samples was obtained from the International Animal Care and Use Committee on Ethics at the Experimental Research Institute of the *Victor Babes* University of Medicine and Pharmacy of Timisoara, Romania. 24 Wistar rats were randomly distributed into the following three groups:

Group A (negative control group).

Group B – to be used with bovine graft material (positive control group).

Group C - to be used with bovine graft material, after the application of LLLT.

The surgical procedure was preceded by an anesthesia with Ketamine (100 mg/kg, Intervet) and Rumpun (10 mg/kg, Bayer Germany) and the preparation of the surgical site (i.e., the region around the scalp was shaved and antisepticised with betadine). A semilunar incision was performed and a full thickness flap was reflected in the anterior direction (Fig. 1). To prevent spontaneous bone healing, a 5 mm calvarial defect was created, by using a trephine burr and a surgical hand piece, under a continuous sterile saline irrigation. To establish the same position of the defect in the rat calvarial region of all rats, a plastic positioning matrix with a circular gap of 5 mm was created; this was used as a surgical guide. Special attention was needed to avoid damaging in any way the dura mater during the surgical procedure.

After creating the surgical calvarial defect, **Groups B and C** received bovine grafting material, whilst **Group A** remained the negative control group, without any grafting material. Periosteum and scalp were sutured in a two layers manner using 6/0 Prolene and 5/0 Prolene for the skin. Cefazoline (100 mg) was given to the animals by intramuscular injections immediately after the surgery for 2 days. After the surgery, the animals were continuously kept at a 22 ± 5°C temperature and at a 50 ± 5% humidity. **Group C** was exposed to LLLT using an own developed protocol using a Gallium - Aluminum – Arsenide laser (GaAlAs) (IRRADIA Mid-Laser® Stockholm, Sweden), emitting at a central wavelength of 808 nm, with an optical power of 450 mW (Fig. 2).

An energy of 2 J/cm^2 was applied immediately after the intervention, as well as every other day until the established sacrifice day was reached. LLLT was performed in 4 points around the defect and in a central point (with a frequency of 3800 Hz, 450 mW, 17 s per point, 18.9 J per

treatment session), which were established and reproduced each time using a plastic positioning matrix manufactured in our group. The animals were distributed into groups according to three healing periods applied after the surgical procedure. In the first group (1) one third of the rats, euthanatized after 14 days were included; another third, euthanatized after 21 days were included in the second group (2), and the rest of rats, euthanatized after 30 days were included in the third group (3). Bone samples were harvested and prepared in such a way that they included the defect along with the surrounding tissues.

A first limitation of the study comes from the fact that the volume of bone assessed originate from different rats, therefore a variation given by the specificity of the healing process of each animal is unavoidable. Considering several rats in each group and performing an average of the results is a method to decrease errors produced by individual variations.

2.2 OCT system

The in-house developed CMS/SS OCT system utilized in the investigations, described in detail in [45] is presented in Fig. 3(a, b), while examples of two rat bone samples imaged with it are shown in Fig. 3(c, d). The galvanometer scanners are driven with a triangular waveform of 2 V voltage peak-to-peak, which corresponds to a 2.8 mm linear scan on the sample. The scanned field (therefore, the Field-of-View (FOV) of the OCT system) is set at the upper possible limit to avoid distortions of the image when the fast scanner is driven at 250 Hz [46]. Therefore, to cover the 5 mm in diameter cylindrical defect situated on the upper part of the bone sample, four individual OCT images are collected, each with a square surface of 2.8×2.8 mm^2, as shown in Fig. 4(a). To study the formation of the new bone inside it - with or without the bovine graft material added to the defect, each of the four quadrants of the defects is imaged separately. The

interface with the original bone is of special interest, in order to study the process of formation of new bone in time.

Examples of OCT images produced during the investigations are presented in Fig. 4(c). The sketch in Fig. 4(b) illustrates the positioning of the four quadrants. A raster scan is obtained by scanning the galvanometers along *x*- and *y*-directions, with the *z*-axis oriented along the depth axis. As it can be observed in Fig. 4(c), three categories of images could be analyzed simultaneously using the in-house CMS developed system and software:

- *A global image* (similar to a coarse confocal image), in the plane *xy* taken from the top of the sample (situated in the bottom left part of the screen), which serves to position the area of interest – in this case the interface between the original and the new formed bone inside the cylindrical defect (as detailed in the following section) in the FOV of the imaging instrument.

- *B-scan/transversal sections* into the sample in the *yz* and *xz* planes (marked with blue and red dashed lines); they can be selected and moved using the two lines shown (with blue and red, respectively) in the *xy* confocal image in the bottom left corner.

- *Nine simultaneously produced xy en-face images (C-scans)*, taken in the *xy* planes, from different equidistant adjustable axial positions from within the sample. The axial depths of the nine *en-face* images are shown on both B-scan images (between the dashed lines).

2.3 Assessment of bone quantities

To utilize the multimodal CMS/SS OCT system for quantitative assessment, the different types of tissue bones have to be distinguished on each *en-face* slide obtained during the imaging process. Brightness thresholds therefore must be assigned to each type of bones, as shown in Fig. 5.

This is easy for the bovine bone particles introduced in the defect for Group B – as these are highly mineralized, therefore easy to distinguish by the brightest zones in all the images. The more difficult assignment of brightness thresholds is for new bone, formed at the margins of the defect zone for Group A as well as at the margins and around the additional bone particles, for Group B.

One may object to the fact that a simple intensity threshold is proposed and applied to the *en-face* OCT images, as they show the tissue at different depths. This is another inherent limitation of the method, but, to our knowledge there is no other way to do the assessment using OCT, but to involve the assumption that the brightness level is indicative to the bone strength, as already accepted in OCT studies of demineralization. OCT shows signal variations within the bone tissue. We interpret these as mineralization differences of trabeculae resulting in different refractive indices causing brighter and darker areas in the imaged bone tissue. This information enables a calculation of the average trabecular mineralization and indicates the direction and velocity of past bone growth in analogy to growth rings of plants [47].

3 Results and discussion

Although in real time only nine *en-face* images are currently displayed on the screen, 600 such images over an axial range of 1.6 mm are produced by the CMS software for the 3D/volumetric reconstruction of the sample, as shown in the examples in Fig. 6 for all the four quadrants marked in Fig. 4(a). Thus, Fig. 5(a) shows the 12 image display from the control group (i.e., from **Group A**) taken after the shortest time interval considered (i.e., 14 days); Fig. 6(b) shows the 12 image display for the additional bone particles in the defect and LLLT throughout the healing period (i.e., from **Group C**), after the longest interval considered (i.e., 30 days) in order

to highlight the differences between a sample with the lowest and the highest quantity of new bone formed, respectively. The contrast between the quantities of the new bone formed in these two extreme situations can be clearly seen when comparing the two sets of images.

The newly bone formation is evaluated by comparison between the three groups, performed at three moments of time: (1) t_1=14, (2) t_2=21, and (3) t_3=30 days (Fig. 7). This shows the 12 image display acquired from the 2.8 × 2.8 mm^2 surface of a quadrant – for each of the samples considered. For clarity, a single sample is shown for each group and at each time moment t_i, i=1,2,3.

According to B-scan images such as those presented in Fig. 7, from the central part of the defect no back-scattered light is collected (especially in the upper part of the sample), whereas towards its periphery a significant number of photons originates from the tissue surface. The further to the periphery of the *en-face* image the deeper the corresponding structure lies. This depends on the surface structure of the sample, but the effect can be quite pronounced. One may therefore point out that the varying signal strengths should be considered, i.e. large number of back-scattered photons from the surface, weaker signal (~exponential decay) from deeper layers. These may also depend on the focus position and shadowing from upper layers, that may influence a signal intensity-based separation of tissue types.

In this respect we must emphasize that the method proposed here does not take into account variations of intensity due to attenuation, absorption and scattering. Scattering and absorption change with depth, but throughout the study we have not attempted to compare brightness from different depths. If comparison would have been done in B-scans, then the contrast change with depth should have been taken into consideration.

As a drawback of the current instrument, due to the surface curvature, the *en-face* information may not be collected from the same depth in all lateral pixels within the *en-face* image. Indeed, we have not corrected for that extra depth dependence due to surface variations, because doing comparisons inside the *en-face* image secures a certain consistency: all pixels at that depth have been affected similarly by the intermediate layers on top (obviously as long as the surface is sufficiently flat).

Also, to minimize errors, the bone sample removed from the rat's calvarial area was positioned as shown in Fig. 3(c, d) and divided into 4 quadrants, which generated OCT images with a surface of only 2.8×2.8 mm^2 each. This has been a way of addressing the issue of the curvature mentioned above. Such images included, in certain situations, a larger quantity of native bone, which could be noticed by the periphery of the artificially created defect. This means that another quadrant has included a larger part of the defect. The investigations, as well as the statistics performed on the data obtained included all four quadrants, and thus, the entire area of interest, including the periphery of the defect, as a way to reduce the errors with regards to the entire sample curvature (as mentioned above) and of the amount of native bone included in certain images.

The same panel presented in Fig. 7 is replicated in Fig. 8, considering the 3D reconstructions of the same bone samples as in Fig. 7. Images show a different appearance of the bone samples, depending on the treatment applied and on the healing time which was established for each animal group. In the control group, the margins of the defect are obvious, being formed of native bone; meanwhile the center of the defect is empty or less representative in bone tissue. In the second group, the center of the defect is filled with bovine graft material, in between of which there is an appearance of newly formed bone tissue. The same appearance, but more

homogenous, is found in the Group C, where laser radiation was applied to the defect filled with grafting material.

We quantified the amount of newly formed bone, using the scheme presented in Fig. 9(a) for the healing of the artificially created defect. The correspondence between the types of bones schematically presented in the sketch in Fig. 9(a) and a real *en-face* OCT image, for a positive and negative control of the sample is shown in Fig. 9(b).

To quantify the newly formed bone, a dedicated software was developed. Its main attribute is to establish ranges for the brightness of different types of bone, and to generate the specific percentage for every category. The use of this program is exemplified in the supplemental material (movie 2). The cursor on the top left image selects an *en-face* OCT image from a specific axial position. Each of the 4 images in the second row has a brightness within the range of values adjustable via the two cursors at the top of each image.

This new bone – which is the target of the entire study, appears throughout the entire 30 days period. However, when it is just formed it is darker (i.e., less mineralized), while as time passes it becomes brighter - as it is more and more mineralized. A brightness interval [$M_{\min}$, $M_{\max}$] therefore has to be defined, with two thresholds (Fig. 5): the lower limit $M_{\min}$ corresponds to the new bone formed after 14 days (i.e., t_1, the shortest time considered), while the upper limit $M_{\max}$ corresponds to the new bone formed after 30 days (i.e., t_2, the longest time interval) – and this latter tissue has the brightness lower than the native bone and also than the bovine bone grafting material.

Using the thresholds pointed out in Fig. 5 and the program developed, each of the N *en-face* OCT image obtained is analyzed and produces the area A_j, $j = 1 \ldots N$ of the new formed bone. As

each *en face* image has a thickness $h \sim 5$ μm into the sample, the volume of the new formed bone can be estimated as:

$$V = h \cdot \sum_{j=1}^{N} A_j \ .$$

With the established thresholds, for all samples, the program thus generates the percentages of every type of bone.

The thresholds utilized are identical or almost identical for all the considered groups. Their variations over the sample volume were small and they were the exception rather than the rule. Such variations were considered only in order to eliminate artefacts in the samples. In no situation such variations led to complete elimination of essential structures of bone tissue from the graphical analysis.

Regarding the curvature of the samples pointed out in the discussion on Fig. 7, in order to minimize such errors, we took into consideration that no segmentation was used. As we compare *en-face* images from a selected depth, if the surface is curved, the substance selected is not from the same depth measured from the top. Because of that, reference to the bone is relative to the cut. To tackle with this issue, we considered several *en-face* images from each quarter of each sample and made the sum for the reflectivity. The software we have developed allows visualization of 196 *en-face* positions for each quarter of the sample. We excluded from our statistical analyze the periphery of the defect, containing only calvaria bone, in order not to influence the results of the study. In this way, we begin the analyze at the margins of the defect, taking into consideration every 10 steps-position, meaning an average of 20 positions for every sample. This generated approximately 60 percentages of different bone types for every sample.

The four results, for the four quarters of each sample were added and we obtained a final number for each type of bone.

We exemplify in Fig. 10 the results obtained in this way. From the point of view of the intensity there are significant differences between the images from the first row of Fig. 10 with regard to the homogeneity of the different intensities. Samples in the control Group A present high intensities at the periphery of the defect and weak or no intensities in the center of the defect, as remarked from the C-scans/*en-face* images. The positive control Group B and the study Group C exhibits a more homogeneous distribution of the intensities, because all samples have defects with (different types of) bone tissue inside.

New bone can be detected at locations where one would expect to see native bone. Regarding this aspect, one must consider that to sustain and maintain bone healing, vascularity and cell distribution specific to this process, the existence of a topographic structure to guide the regeneration and mineralization is necessary. This is the reason why in the defects left empty for healing, this process starts from the periphery towards the center of the defect. The new bone is therefore produced in the vicinity of the native, well-mineralized one. In defects where the guided regeneration is conducted via different types of bone particles, these particles act as a support to initiate the bone formation. In this case new bone can be noticed not only at the periphery of the defects, but also in the central part of the bone formation placed in connection with additional bone particles. Regarding the superposition of the artificial bone particles with the native bone, two aspects must be taken into account: (i) the defects created in the animals' calvarial area were left to be healed *in vivo*, in which case some dynamics is evident, as different local movements of the artificial bone occur (as it is also the case of human subjects); (ii) because of the bone reshaping and resorption processes that always take place in the initial step

of the healing, artificial bone has to be used in excess in the defect. It is therefore possible for artificial bone particles from the interior of the defect to reach the periphery of the defect, where native bone exists. One can notice in Fig. 10 that on all images taken into consideration all three types of bone are present: native, artificial, and newly formed (less mineralized) bone. This can also be noticed from Fig. 7, but only the analyze in Fig. 10 highlights the different types of bone, after using the programme developed.

An additional aspect refers to the speckles that fully modulate the OCT intensity signal. These have not been accounted for by spatial averaging in Fig. 10. in order to avoid reducing the sharpness. However, the evaluations themselves involved some average process anyway. We did not look at a single point in the *en-face*, where the effect of the speckle may only be mitigated by weighed averaging of multiple *en-face* images produced at different moments, but we added up the brightness of a collection of points.

Using the data obtained, a statistical analysis of the results was performed, using ANOVA and Tukey tests. The results of the analysis are presented in Figs. 11 and 12.

The statistical analysis highlights the information obtained regarding the healing curve of the bone tissue: by performing a comparison between the three study groups, the results showed significant differences in the healing process depending on the time of healing and also on the treatment applied. The statistics calculations have included all the values obtained in order to improve the errors as much as possible. Out of 600 *en-face* images produced we selected 40 images for each sample, positioned taking into account the specific depth of each sample, as remarked from the B-scan provided by the system. A full coverage of the entire depth of the defect was provided this way.

As it can be concluded from Fig. 11, differences with statistical significance were found between the two control groups, positive B and negative A. The percentage of newly formed bone was higher for the healing period of 30 days than for 21 or 14 days, both for negative control Group A (in which defects healed spontaneously) and for the positive control Group B (in which bovine bone graft was added to the defect).

Moreover, the most important variation was found by performing a comparison between Groups B and C, thus evaluating the effect of LLLT on the healing process of the bone tissue. Significant differences were found throughout the statistical analysis for the healing period of 21 days, where it seems that the laser radiation had the highest effect, by inducing the formation of the highest quantity of new bone (see the results for V and VI – Figs. 11 and 12). We should also take into consideration that laser photo-biomodulation effect does not happen immediately, as it is known to be a cumulated effect, therefore it may appear by the end of the assessment period. The results obtained using OCT were confirmed when performing the histological examination of the samples - Fig. 13(a, b).

The ground truth obtained by histology demonstrates that the images shown in Fig. 10 represent the claimed tissue types. Proximity of particles of artificial bone to native bone or newly formed bone represents a normal healing process, which is well-known and demonstrated in the literature. This comes from the fact that particles of artificial bone are utilized in bone augmentation, not only to compensate for the loss of bone tissue, but also in order to form a topographic structure on which the process of bone growth can occur; this is essential for large defects.

The results obtained in our study suggest that positive effects of LLLT on the bone repair processes are time dependent, being more obvious during the initial phases of the healing (Figs.

11 and 12). This conclusion is also supported by the findings of other research groups, which have used other investigation methods than OCT [22-24]. Qualitative histological analysis and histometric analysis showed that LLLT can improve bone formation process in rat calvarial defects filled or not with bovine bone graft, but it is not able to accelerate particles resorption of this material in the interior of bone defect [48]. Levels of calcium, phosphorus, and protein can also be determined by using atomic absorption spectrometry, colorimetry, and photometry when investigating possible effects of LLLT on bone formation [49].

In another study, the histological evaluation showed a statistically significant increase in new bone formation of LLLT group relative to the control ($P < 0.05$). In addition, inflammation was significantly reduced in the LLLT group compared to the control [50]. The histological evaluation still represents the gold standard, being relevant in assessing inflammatory infiltration, trabecular bone matrix, periosteal, and new bone formation [51]. Although having a significant importance, the histological assessment is invasive, which does not allow any further examinations on the same samples. In contrast to using these other methods, the present study demonstrates the capability of OCT to assess newly formed bone, both qualitatively and quantitatively, while the histological analysis has confirmed the findings obtained using OCT.

4 Conclusions

A quantitative analysis of the process of bone formation in rat calvaria was achieved using OCT. Such studies are essential to assess the efficiency of different techniques that can be used in bone regeneration, especially taking into consideration the complexity of the wound healing process and the large number of factors influencing it.

Multimodal CMS/SS OCT was applied to image and analyze the different groups considered in order to assess the new bone formation process: negative control Group A, positive control Group B (with additional bone), and Group C (with additional bone and LLLT). Imaging the bone defect on quadrants and using C-scans/*en-face* images (as well as B-scans and confocal images), statistically consistent conclusions were extracted from the study. Essentially, Group C was demonstrated to have more new formed bone than Group B, which had more new bone than Group A. By analyzing the evolution of the quantity of new bone in time (by performing the euthanasia of the rats after three time intervals, i.e. after 14, 21, and 30 days), the most significant difference between these quantities of new bone was after 21 days, therefore approximately after two thirds of the total time interval analyzed. After the longer time considered, the quantities of bone tend to move closer, which is logical, as they begin to fill the available gap. Histological images were included in the study, to demonstrate the validity of the assumptions made regarding the different types of bone identified in the study.

To our knowledge, this is the first time when OCT is employed as a tool to assess the effects of laser photo-biomodulation on bone regeneration. Despite inherent limitations of the method, the results obtained and the statistics performed using OCT were in good agreement with previous studies that approached new bone formation using other methods, including histology. As such, we believe that this work represents a progress towards bone formation studies using *en-face* imaging.

Future work includes the application of LLLT to enhance the bone regeneration using different protocols and parameters. All the data available in the literature reveal that the efficiency of the therapy is affected by the dosage, irradiation time, and mode. Regarding measurable effects, it seems that LLLT is more effective when applied in the early stages of the wound healing,

probably due to the high cellular proliferation rate. The increase in vascularity and the response of the osteoblasts remain important aspects to be taken into consideration when assessing LLLT effects. Similar future studies may be considered to target the effect of LLLT on cellular differentiation and growth, especially regarding mesenchymal stem cells and mesenchymal stromal cells therapies, during what nowadays is known as regenerative medicine.

Disclosures

The authors have no relevant financial interests in the manuscript and no other potential conflicts of interest to disclose.

Acknowledgments

Romanian National Authority for Scientific Research (CNDI–UEFISCDI) (PN-III-P2-2.1-BG-2016-0297, http://3om-group-optomechatronics.ro/); European Union through the European Regional Development Fund, the Competitiveness Operational Program (BioCell-NanoART, Grant POC-A1-A1.1.4-E nr. 30/2016). Adrian Bradu and Adrian Podoleanu also acknowledge the support of the Engineering and Physical Sciences Research Council (EPSRC) ('REBOT', EP/N019229/1). Adrian Podoleanu is also supported by the H2020 European Research Council (ERC) ('ADASMART', 754695), National Institute for Health Research Biomedical Research Centre at Moorfields Eye Hospital NHS Foundation Trust (NIHR) and UCL Institute of Ophthalmology, University College London, the Royal Society Wolfson Research Merit Award.

References

1. Ashman A. Postextraction ridge preservation using synthetic alloplast. Implant Dent 2000; 9: 168-76.
2. Toscano N, Shumaker N, and Holzclaw D. The art of block grafting – A review of the surgical protocol for reconstruction of alveolar ridge deficiency. The J. of Implant and Advanced Clin. Dent. 2000; 2: 45-66.
3. Chiapasco M and Zaniboni M. Bone augmentation procedures in implant dentistry. The International J. of Oral and Maxillofacial Implants 2009; 24: 237-59.
4. Boyce T, Edwards J, and Scarborough N. Allograft bone: the influence of processing on safety and performance. Orthop. Clin. North Am. 1999; 30: 571-81.
5. Giannoudis PV, Dinopoulos H, and Tsiridis E. Bone substitutes:An update. Injury. Int. J. Care injured 2005; 36S: S20-S27.
6. Karageorgiou V and Kaplan D. Porosity of 3D biomaterial scaffolds and osteogenesis. Biomaterials 2005; 26: 5474-91.
7. Thaller SR, Hoyt J, Dart A, Borjeson K, and Tesluk H. Repair of experimental calvarial defects with Bio-Oss particles and colagen sponges in a rabbit model. J. Craniofac. Surg. 1994; 5: 242-6.
8. Accorsi-Mendonca T, Conz MB, Barros TC, de Sena LA, Soares G, and Granjeiro JM. Psycochemical characterization of two deproteinized bovine xenografts. Braz. Oral Res. 2008; 22: 5-10.
9. Simion M, Fontana F, Rasperini G, and Maiorana C. Vertical ridge augmentation by expanded-polytetrafluoroethylene membrane and a combination of intraoral autogenous bone

graft and deproteinized anorganic bovine bone. Bio. Oss. Clin. Oral Implants Res. 2007; 18: 620-9.

10. Renno ACM, McDonnell PA, Parizotto NA, and Laakso EL. The effects of laser irradiation on osteoblast and osteosarcoma cell proliferation and differentiation *in vitro.* Photomed. Laser Surg. 2007; 25: 275-80.
11. Stein A, Benayahu D, Maltz L, and Oron U. Low-level laser irradiation promotes proliferation and differentiation of human osteoblasts *in vitro.* Photomed. Laser Surg. 2005; 23: 161-6.
12. Barbosa D, de Souza RA, Xavier M, da Silva FF, Arisawa EA, and Villaverde AGJB, Effects of low-level laser therapy (LLLT) on bone repair in rats: optical densitometry analysis. Lasers Med. Sci. 2013; 28: 651–6.
13. Cunha MJS, Esper LA, Sbrana MC, de Oliveira PGFP, do Valle AL, and de Almeida ALPF. Effect of Low-Level Laser on Bone Defects Treated with Bovine or Autogenous Bone Grafts: In Vivo Study in Rat Calvaria. BioMed Research International 2014; Article ID 104230.
14. da Silva RV and Camilli JA. Repair of bone defects treated with autogenous bone graft and low-power laser. J. of Craniofacial Surgery 2006; 17: 297–301.
15. Ueda Y and Shimizu N. Effects of pulse frequency of low-level laser therapy (LLLT) on bone nodule formation in rat calvarial cells. J. Clin. Laser Med. Surg. 2003; 21: 271–77.
16. Coombe AR, Ho CTG, Darendeliler MA, Hunter N, Philips JR, Chapple CC, and Yum LW. The effects of low-level laser irradiation on osteoblastic cells. Clin. Orthop. Res. 2001; 4: 3–14.

17. Garcia VG, da Conceição JM, Fernandes LA, de Almeida JM, Nagata MJH, Bosco AF, and Theodoro LH. Effects of LLLT in combination with bisphosphonate on bone healing in critical size defects: a histological and histometric study in rat calvaria. Lasers Med. Sci. 2013; 28: 407–14.
18. Silva Júnior AN, Pinheiro AL, Oliveira MG, Weismann R, Ramalho LM, and Nicolau RA. Computerized morphometric assessment of the effect of LLLT on bone repair: an experimental animal study. J. Clin. Laser Med. Surg. 2002; 20: 83–7.
19. Kipshidze N, Nikolaychic V, Keelan MH, Shankar LR, Khanna A, Kornowski R, Leon M, and Moses J. Low power helium: neon laser irradiation enhances production of vascular endothelial growth factor and promotes growth of endothelial cells in vitro. Lasers Surg. Med. 2001; 28: 355–64.
20. Luger EJ, Rochkind S, Wollman Y, Kogan G, and Dekel S. Effect of low power laser irradiation on the mechanical properties of bone fracture healing in rats. Lasers Surg. Med. 1998; 22: 97–102.
21. Pyczek M, Sopala M, and Dabrowski Z. Effect of low energy laser power on the bone marrow of the rat. Folia Biol. 1994; 42: 151–6.
22. Pinheiro AL and Gerbi ME. Photoengineering of bone repair processes.Photomed. Laser Surg. 2006; 24: 169–78.
23. Vladimirov YA, Osipov AN, and Klebanov GI. Photobiological principles of therapeutic applications of laser radiation. Biochemistry 2004; 69: 81–90.
24. Brugnera AJr, dos Santos AE, Garrin C, Bologna ED, Ladalardo TC, Pinheiro LP. *Atlas of Applied laser therapy to clinical dentistry, Prospects in the use of therapeutic laser,* 2006.

25. Ribeiro TP, Nascimento SB, Cardoso CA, Hage R, Almeida JD, and Loschiavo Arisawa EA. Low-Level Laser Therapy and Calcitonin in Bone Repair: Densitometric Analysis. International Journal of Photoenergy 2012; Article ID 829587.
26. Deniz E, Arslan A, Diker N, Olgac V, and Kilic E. Evaluation of light-emitting diode photobiomodulation on bone healing of rat calvarial defects. Biotechnology & Biotechnological Equipment 2015; 29: 758-65.
27. Park SY, Kim K-H, Koo K-T, Lee K-W, Lee Y-M, Chung C-P, and Seol Y-J. The evaluation of the correlation between histomorphometric analysis and micro-computed tomography analysis in AdBMP-2 induced bone regeneration in rat calvarial defects. J. Periodontal Implant Sci. 2011; 41: 218-26 .
28. Huang D, Swanson EA, Lin CP, Schuman JS, Stinson WG, Chang W, Hee MR, Flotte T, Gregory K, Puliafito CA, and Fujimoto JG. Optical coherence tomography. Science 1991; 254: 1178-81.
29. Drexler W, Liu M, Kumar A, Kamali T, Unterhuber A, and Leitgeb RA. Optical coherence tomography today: speed, contrast, and multimodality. J. Biomed. Opt. 2014; 19: 071412.
30. Feldchtein F, Gelikonov V, Iksanov R, Gelikonov G, Kuranov R, Sergeev A, Gladkova N, Ourutina M, Reitze D., and Warren J. *In vivo* OCT imaging of hard and soft tissue of the oral cavity. Opt. Express 1998; 3: 239-50.
31. Podoleanu A Gh and Rosen RB. Combinations of techniques in imaging the retina with high resolution. Progress in Retinal and Eye Research 2008; 27: 464-99.
32. Lee K-S, Zhao H, Ibrahim SF, Meemon N, Khoudeir L, and Rolland J. P. Three-dimensional imaging of normal skin and nonmelanoma skin cancer with cellular resolution using Gabor domain optical coherence microscopy. J. Biomed. Opt. 2012; 17:126006.

33. Jones RS, Staninec M, and Fried D. Imaging artificial caries under composite sealants and restorations. J. Biomed. Opt. 2004; 9: 1297-304.

34. Queiroz de Melo Monteiro G, Montesa MAJR, Gomes ASL, Motac CBO, Sérgio L, and Freitas AZ. Marginal analysis of resin composite restorative systems using optical coherence tomography. Dent. Mat. 2011; 27: 213–23.

35. Canjau S, Todea C, Negrutiu ML, Sinescu C, Topala FI, Marcauteanu C, Manescu A, Duma V-F, Bradu A, and Podoleanu A. Gh. Optical Coherence Tomography for Non-Invasive ex vivo Investigations in Dental Medicine - a Joint Group Experience (Review). 2015; STM ∫: 7: 97-114.

36. Oancea R, Bradu A, Sinescu C, Negru RM, Negrutiu ML, Antoniac I, Duma V-F, and Podoleanu A. Gh. Assessment of the sealant/tooth interface using optical coherence tomography. J. of Adhesion Science and Technology 2015; 29: 49-58.

37. Adler DC, Chen Y, Huber R, Schmitt J, Connolly J, and Fujimoto J. G. Three-dimensional endomicroscopy using optical coherence tomography. Nature Photonics 2007; 1: 709–16.

38. Dsouza R, Subhash H, Neuhaus K, Kantamneni R, McNamara PM, Hogan J, Wilson C, and Leahy M. Assessment of curing behavior of light-activated dental composites using intensity correlation based multiple reference optical coherence tomography. Lasers Surg. Med. 2016; 48 77–82.

39. Dikshit S, Grover HS, Bhardwaj A and Saini R, Optical Coherence Tomography - A Boon for Dental Diagnostics. British Biomed. Bulletin 2015; 3: 239-52.

40. Santin SP, Ubirajara Santos LA, Zanardi de Freitas A, Martinho Junior AC, Dias DB, Soares FAN, Pino ES, Noronha Veloso M, and Mathor MB. Comparison between optical coherence

tomography technique and mechanical compression assay to evaluate ionizing radiation effects in frozen and lyophilized bone tissue. INAC 2013.

41. Rashidifard C, Vercollone C, Martin S, Liu B, and Brezinski ME. The application of optical coherence tomography in musculoskeletal disease. Arthritis 2013; Article ID 563268.
42. Ionita I. Optical coherent tomography imaging usefulness in implant tissue study.Romanian Reports in Physics 2009; 61: 575–80.
43. Sanda M, Shiota M, Imakita C, Sakuyama A, Kasugai S, and Sumi Y. The effectiveness of optical coherence tomography for evaluating peri-implant tissue: A pilot study. Imaging Science in Dentistry 2016; 46: 173-8.
44. Negruţiu ML, Sinescu C, Canjau S, Manescu A, Topala FI, Hoinoiu B, Romînu M, Marcauţeanu C, Duma V-F, Bradu A, and Podoleanu A Gh. Bone regeneration assessment by optical coherence tomography and MicroCT synchrotron radiation. Proc. SPIE 2013; 8802: 880204.
45. Podoleanu A Gh and Bradu A. Master–slave interferometry for parallel spectral domain interferometry sensing and versatile 3D optical coherence tomography. Opt. Express 2013; 21: 19324–38.
46. Duma V-F, Laser scanners with oscillatory elements: Design and optimization of 1D and 2D scanning functions. Appl. Mathematical Modelling 2019; 67(3): 456-476.
47. Kasseck C, Kratz M, Torcasio A, Gerhardt NC, van Lenthe H, Gambichler T, Hoffmann K, Jones D, Hofmann MR. Comparison of optical coherence tomography, microcomputed tomography, and histology at a three-dimensionally imaged trabecular bone sample. J. Biomed. Opt. 2010; 15: 046019.

48. Bosco AF, Faleiros PL, Carmona LR, Garcia VG, Theodoro LH, de Araujo NJ, Hitomi Nagata MJ, Milanezi de Almeida J. Effects of low-level laser therapy on bone healing of critical-size defects treated with bovine bone graft. J. of Photochemistry & Photobiology, B: Biology 2016; 163: 303–10.
49. Khadra M, Kasem N, Haanæs HR, Ellingsen JE, and Lyngstadaas SP, Enhancement of bone formation in rat calvarial bone defects using low-level laser therapy. Oral Surgery, Oral Medicine, Oral Pathology, Oral Radiology and Endodontology 2004; 97; 693-700.
50. Fekrazad R, Sadeghi Ghuchani M, Eslaminejad MB, Taghiyar L, Kalhori KAM, Pedram MS, Shayan AM, Aghdami N, and Abrahamse H, The effects of combined low level laser therapy and mesenchymal stem cells on bone regeneration in rabbit calvarial defects. J. of Photochemistry and Photobiology B: Biology 2015; 151: 180–5.
51. Sella V, Bomfim F, Machado PCD, Morsoleto MJ, Chohfi M, and Plaple H. Effect of low-level laser therapy on bone repair: a randomized controlled experimental study. Lasers Med. Sci. 2015; 30: 1061-8.

Caption List

Fig. 1 Steps taken during the surgery phase: full thickness flap elevated (a); creation of a 5 mm diameter defect under continuous cooling (b, c, d, e); insertion of the bovine bone grafting material (f) and of the collagen membrane (g); suture in two layers manner using absorbable (for the first layer) and non-absorbable suture (for the second layer) (h, i).

Fig. 2 Group C is exposed to LLLT, using a GaAlAs laser (IRRADIA Mid-Laser® Stockholm, Sweden), in 4 points around the defect as well as in a central point, which were established and reproduced each time using a plastic positioning matrix. Examples of harvested samples: control Group (A), negative study Group (B), and positive study Group (C).

Fig. 3 (a) Schematic of the in-house developed multimodal CMS/SS OCT system centered at 1300 nm. SS, swept source; DC1-2, directional coupler; MO1-3, microscope objectives; M1-2, flat mirrors; GXY, galvo-scanning head; SL, telecentric scanning lens; BPD, balanced photo-detector; (b) photo of the OCT set-up; (c, d) metal frame for location of the area investigated on the sample.

Fig. 4 (a) Sample to be imaged (i.e., upper part of the skull fragment of the rat – with cylindrical defect) showing the same notations for the four quadrants considered as in Fig. 4; (b) dimensions and orientation of the volumetric OCT reconstruction; (c) 12 image display of delivered by the CMS SS-OCT software. The size of each *en face* OCT image and of the confocal one is 2.8 × 2.8 mm^2. The size of the two orthogonal B-scan images is 1.6 × 2.8 mm^2. The *en-face* OCT images are separated by 42.56 μm. The first *en-face* OCT image corresponds to z = 0.4 mm within the specimen. All distances are measured in air.

Fig. 5 Thresholds of the brightness *M* of the different types of bone tissue – considered in order to evaluate the quantity *Q* of new formed bone.

Fig. 6 (movie 1). 12 image view for a pair of images formed from Group A (after t_1=14 days) and Group C (additional bone after t_3=30 days). The movie shows the pair of images for each of the 4 quadrants (i) to (iv) according to notation in Fig. 4(a). Each *en-face* OCT image has a square surface (in the *xy* plane) of 2.8 × 2.8 mm^2. The image frozen here is that of the pair of 12 image view for quadrant (iii). The first *en-face* displayed is collected at a depth z = 0.4 mm, while the distance between the displayed *en-face* images is 42.56 μm. The axial range of the two B-scan images is 1.6 mm. All distances are measured in air.

Fig. 7 Monitoring the process of new bone formation for the three Groups A, B. and C - after (1) t_1=14 days, (2) t_2=21 days, and (3) t_3=30 days. The upper left quadrant (ii) of each sample has been considered (please see Fig. 4(a)). Each *en-face* OCT image has a square surface (in the *xy* plane, see Fig. 4) of 2.8 × 2.8 mm^2. The first *en-face* displayed is collected at a depth z = 0.4 mm, while the distance between the displayed *en-face* images is 42.56 μm. The axial range in the B-scan images is 1.6 mm.

Fig. 8 The same study as in Fig. 7, showing OCT 3D reconstructions of the upper left quadrant of the samples for each group, A, B and C after (1) t_1=14 days, (2) t_2=21 days, and (3) t_3=30 days.

Fig. 9 (a) Scheme of the bone defect; (b) different types of bone inside the defect, using OCT imaging.

Fig. 10 Collage of *en-face* images showing different bone structure in the images obtained using OCT scans: bone healing representation for the negative control Group A (a) (at 14 days, 21 days, 30 days), for the positive control Group B (b) (at 14 days, 21 days, 30 days) and for experimental Group C (c) (at 14 days, 21 days, 30 days). The percentage of each type of bone is indicated on each *en-face* OCT each image.

Fig. 11 Mean values and standard deviations for the representation of native bone, bovine bone, and newly formed bone graft in the studied groups, numbered from I to IX, depending on the healing time and on the type of treatment applied:

I: negative control Group A, time of healing 30 days (defect healed spontaneously);

II: positive control Group B, time of healing 30 days (defect filled with bovine bone graft);

III: study Group C, time of healing 30 days (defect filled with bovine bone graft; laser radiation was applied);

IV: negative control Group A, time of healing 21 days (defect healed spontaneously);

V: positive control Group B, time of healing 21 days (defect filled with bovine bone graft);

VI: study Group C, time of healing 21 days (defect filled with bovine bone graft; laser radiation was applied);

VII: negative control Group A, time of healing 14 days (defect healed spontaneously);

VIII: positive control Group B, time of healing 14 days (defect filled with bovine bone graft);

IX: study Group C, time of healing 14 days (defect filled with bovine bone graft; laser radiation applied).

Fig. 12 Comparison between the three study groups regarding the newly formed bone, with significance from a statistical point of view ($P < 0.05$).

Fig. 13 Masson trichrome staining 10×, demonstrating different results for (a) group V (positive control Group B, time of healing 21 days, defect filled with bovine bone graft), and (b) group VI (study Group C, time of healing 21 days, defect filled with bovine bone graft; laser radiation was applied). A few inflammatory cellular elements, homogeneous eosinophilic material crossed with fibrous tissue in a small amount (about 2:1 ratio) and suture material granulomas is presented in (a). Osteoid lamellae (*) that tend to bind bone tissue to eosinophilic material

(which is represented by the bovine bone graft) are presented in (b), where some of the bone lamellae are focally delimited by osteoblasts.

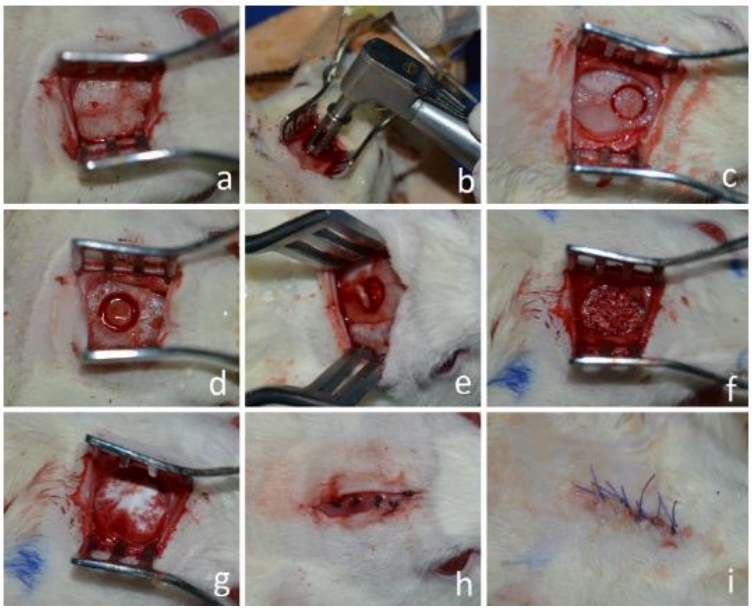

Fig. 1

(a)  (b) 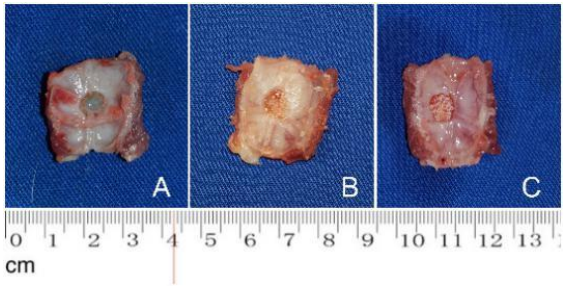

Fig. 2

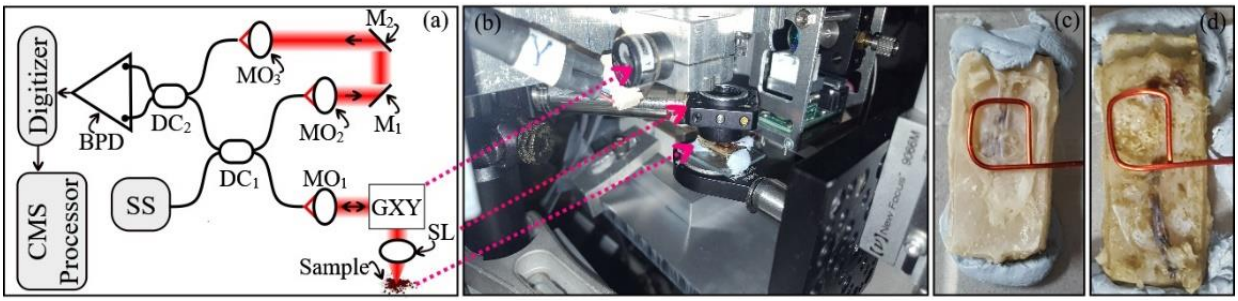
(a)
(b)
(c)
(d)
Digitizer
BPD
DC2
MO3
M2
MO2
M1
DC1
MO1
GXY
SL
SS
CMS Processor
Sample

Fig. 3

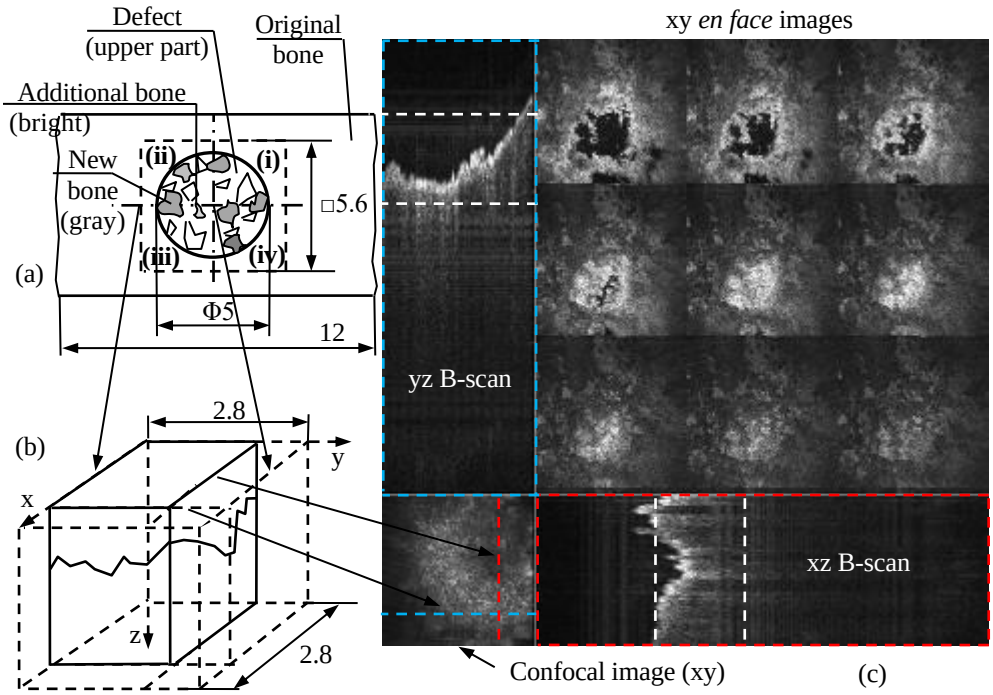
Defect
(upper part)
Original
bone
Additional bone
(bright)
New
bone
(gray)
(ii)
(i)
(iii)
(iv)
□5.6
(a)
Φ5
12
2.8
(b)
y
x
z
2.8
xy *en face* images
yz B-scan
xz B-scan
Confocal image (xy)
(c)

Fig. 4

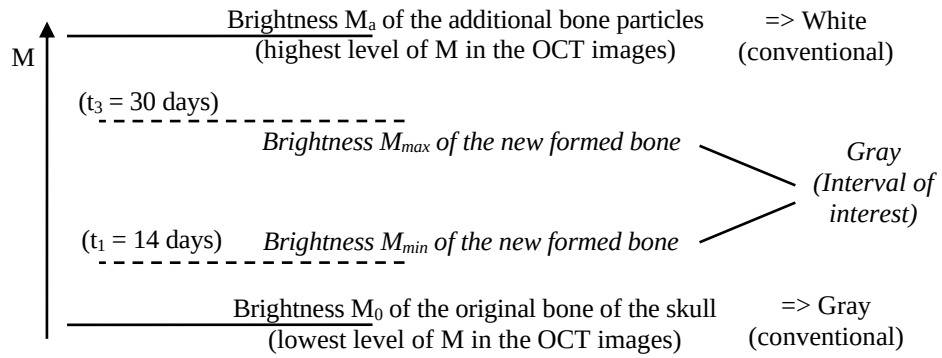
M
Brightness M_a of the additional bone particles
(highest level of M in the OCT images)
=> White
(conventional)
(t_3 = 30 days)
Brightness M_{max} of the new formed bone
Gray
(Interval of interest)
(t_1 = 14 days)
Brightness M_{min} of the new formed bone
Brightness M_0 of the original bone of the skull
(lowest level of M in the OCT images)
=> Gray
(conventional)

Fig. 5

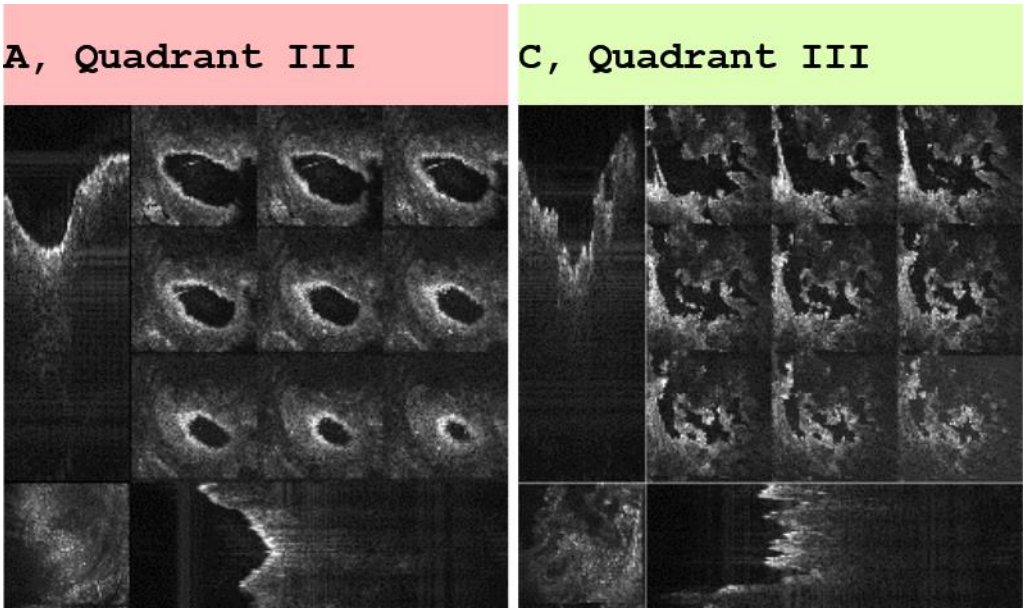

Fig. 6 (movie 1)

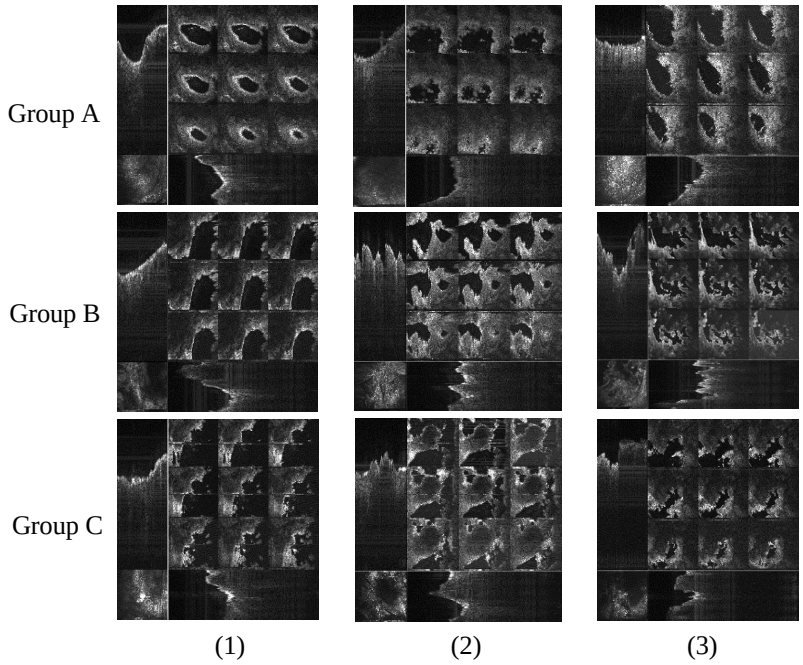

Fig. 7

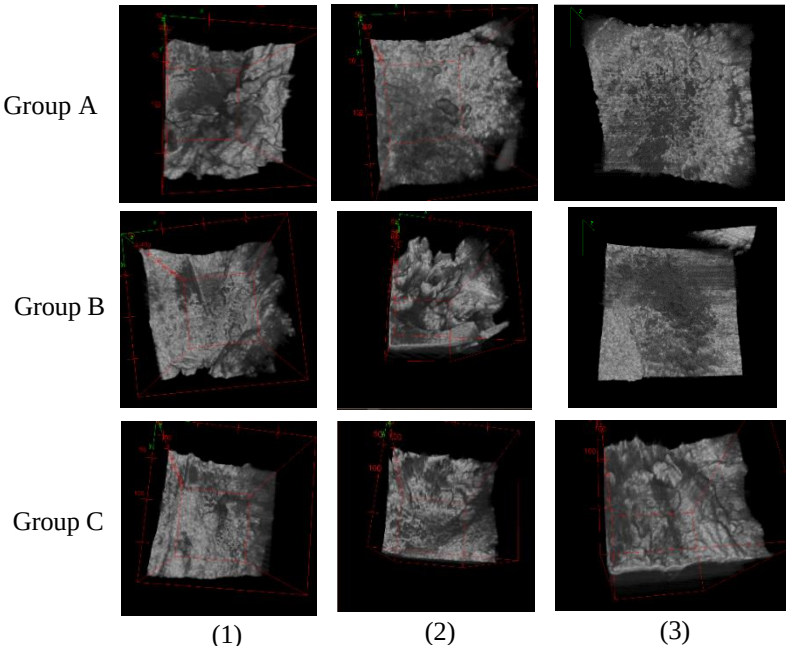

Fig. 8

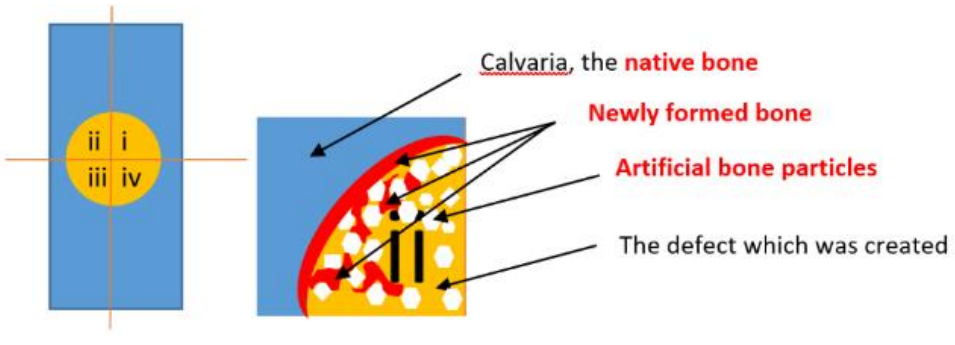
ii i
iii iv
Calvaria, the native bone
Newly formed bone
Artificial bone particles
The defect which was created

(a)

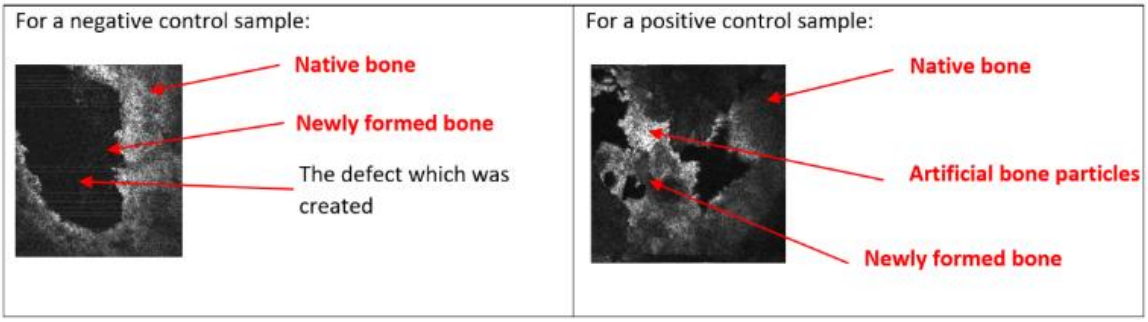
For a negative control sample:
Native bone
Newly formed bone
The defect which was created
For a positive control sample:
Native bone
Artificial bone particles
Newly formed bone

(b)

Fig. 9

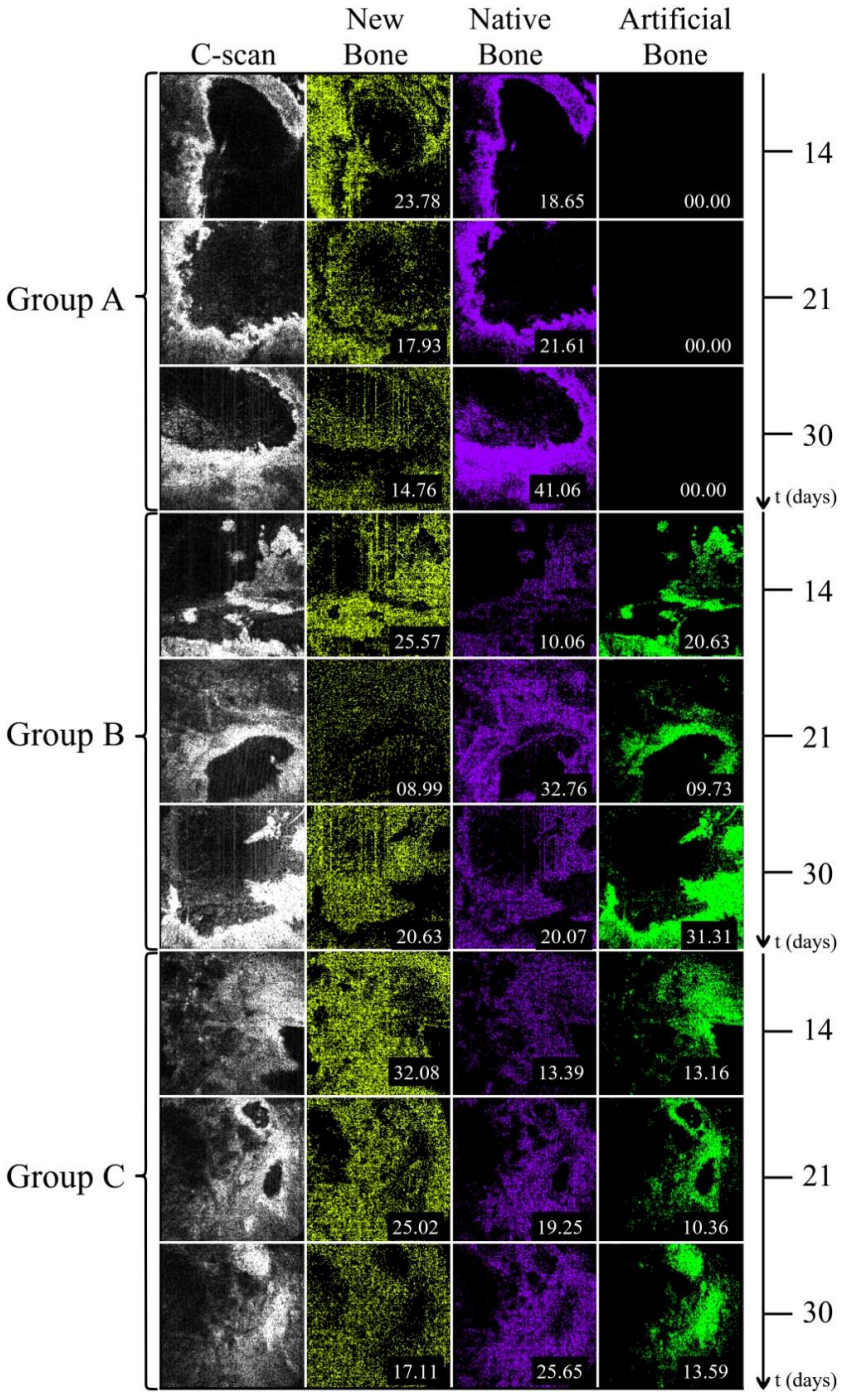
C-scan
New Bone
Native Bone
Artificial Bone
Group A
Group B
Group C
23.78
18.65
00.00
17.93
21.61
00.00
14.76
41.06
00.00
25.57
10.06
20.63
08.99
32.76
09.73
20.63
20.07
31.31
32.08
13.39
13.16
25.02
19.25
10.36
17.11
25.65
13.59
14
21
30
t (days)

Fig. 10

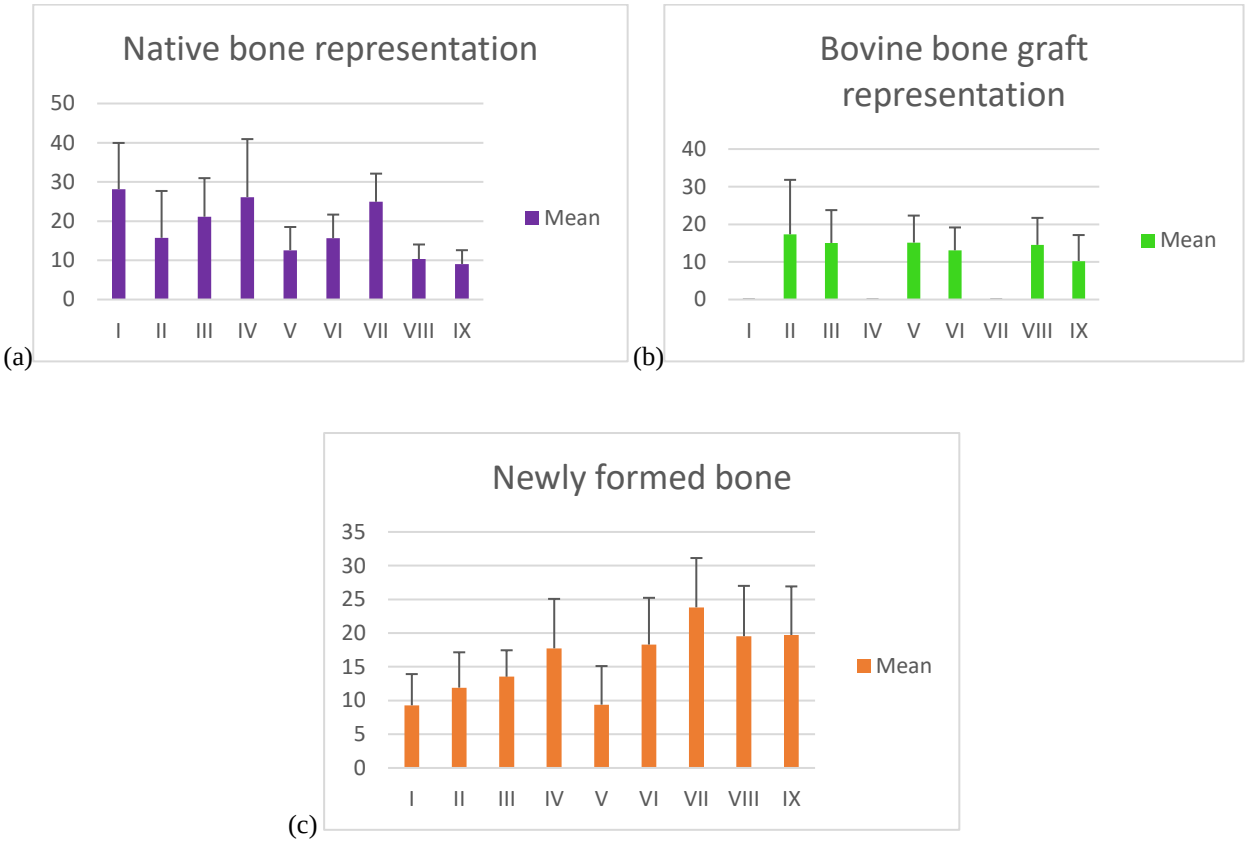
Native bone representation
50
40
30
20
10
0
I II III IV V VI VII VIII IX
Mean
(a)
Bovine bone graft representation
40
30
20
10
0
I II III IV V VI VII VIII IX
Mean
(b)
Newly formed bone
35
30
25
20
15
10
5
0
I II III IV V VI VII VIII IX
Mean
(c)

Fig. 11

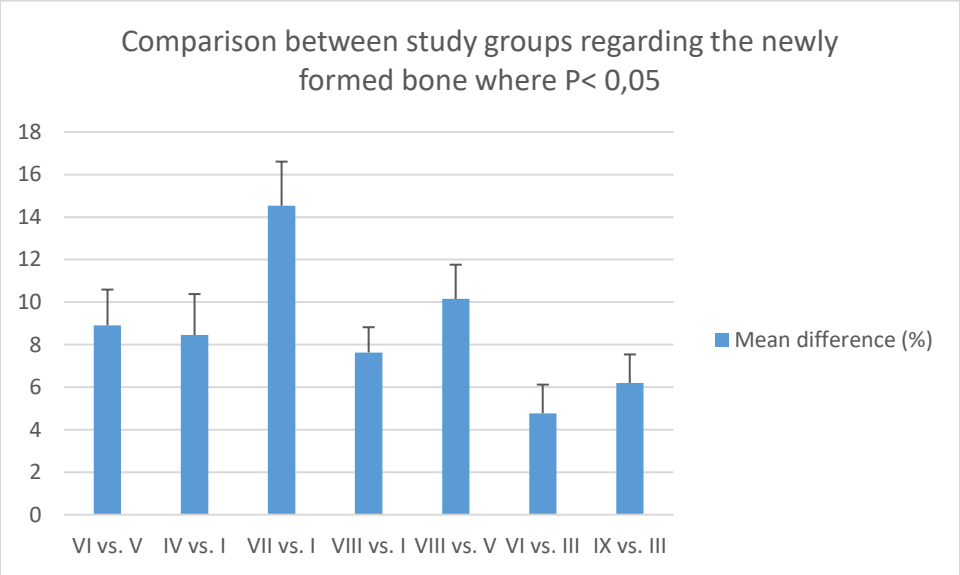
Comparison between study groups regarding the newly formed bone where P< 0,05
18
16
14
12
10
8
6
4
2
0
VI vs. V
IV vs. I
VII vs. I
VIII vs. I
VIII vs. V
VI vs. III
IX vs. III
Mean difference (%)

Fig. 12

(a) 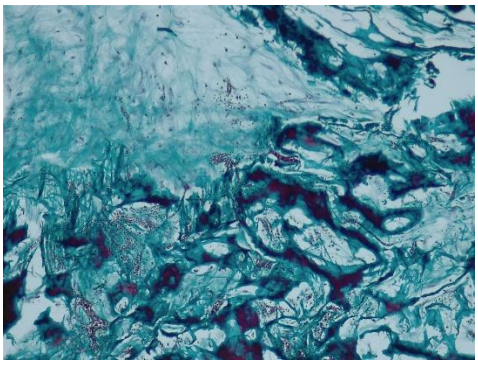 (b) 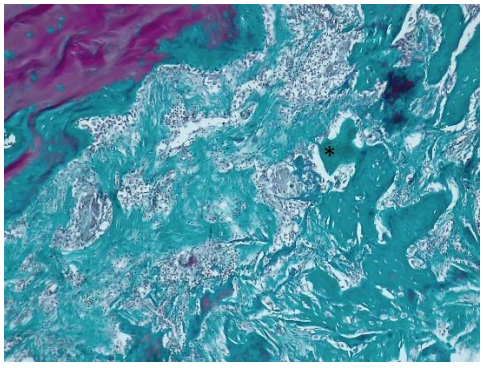

Fig. 13